Quantitative Analysis of Ezrin Turnover Dynamics in the Actin Cortex

Marco Fritzsche,[†‡] Richard Thorogate,[‡] and Guillaume Charras[‡§*]

[†]Department of Physics and Astronomy, [‡]London Centre for Nanotechnology, and [§]Department of Cell and Developmental Biology, University College London, London, United Kingdom

ABSTRACT   Proteins of the ERM family (ezrin, moesin, radixin) play a fundamental role in tethering the membrane to the cellular actin cortex as well as regulating cortical organization and mechanics. Overexpression of dominant inactive forms of ezrin leads to fragilization of the membrane-cortex link and depletion of moesin results in softer cortices that disrupt spindle orientation during cytokinesis. Therefore, the kinetics of association of ERM proteins with the cortex likely influence the timescale of cortical signaling events and the dynamics of membrane interfacing to the cortex. However, little is known about ERM protein turnover at the membrane-cortex interface. Here, we examined cortical ezrin dynamics using fluorescence recovery after photobleaching experiments and single-molecule imaging. Using multiexponential fitting of fluorescence recovery curves, we showed that ezrin turnover resulted from three molecular mechanisms acting on very different timescales. The fastest turnover process was due to association/dissociation from the F-actin cortex, suggesting that ezrin acts as a link that leads to low friction between the membrane and the cortex. The second turnover process resulted from association/dissociation of ezrin from the membrane and the slowest turnover process resulted from the slow diffusion of ezrin in the plane of the membrane. In summary, ezrin-mediated membrane-cortex tethering resulted from long-lived interactions with the membrane via the FERM domain coupled with shorter-lived interactions with the cortex. The slow diffusion of membranous ezrin and its interaction partners relative to the cortex signified that signals emanating from membrane-associated ezrin may locally act to modulate cortical organization and contractility.

INTRODUCTION

Many signaling molecules and regulatory proteins localize to the cell membrane, making it a focal point for the generation, organization, and dynamics of the actin cortex, and therefore for cell morphogenesis. Arguably the best characterized membrane-cortex linkers are proteins of the ezrin-radixin-moesin (ERM) family. Their tethering role is most evident in cell blebs where they are recruited to the membrane before cortex formation (1). Perturbation of ezrin function through expression of dominant negative forms lacking an F-actin binding domain leads to fragilization of membrane-cortex linking and delamination of the membrane from the actin cortex (1). In addition to this mechanical role, ERM proteins act as integrators of signals at the cortex where they can regulate RhoGTPases and cell polarity (2–4). In epithelial cells, ezrin localization to the apical cortex leads to the formation of microvilli and membrane ruffles through ezrin binding of the RhoGEF PLEKHG6 and subsequent activation of RhoG (5). Ezrin activation has been reported to promote cell migration through recruitment of the RhoGEF Dbl and activation of cdc42 (6). In lymphocytes and amoeboid blebbing cells, ezrin is recruited to the cell rear, where it appears to play a role in specifying backness (7–9) and in inducing contractility downstream of

Rho-ROCK through recruitment of Dbl (7). In cultured cells, moesin knockdown results in softening of the cortex that impedes proper spindle alignment and anaphase B (10,11), whereas in mice, a decrease in moesin expression can disrupt epidermal embryogenesis due to defects in spindle orientation and asymmetric divisions (12). Conversely, depletion of a negative regulator of moesin phosphorylation, PP1-89B, leads to an increase in cortex rigidity (13,14).

In its inactive state, ezrin exists in an autoinhibited configuration due to intramolecular interactions of its N-terminal FERM domain (N-ERMAD) with its C-terminal actin-binding domain (C-ERMAD). Inactive ezrin proteins in their closed conformation can form oligomers through N-ERMAD-C-ERMAD intermolecular interactions, and these oligomers can localize either to the cytoplasm or to the membrane (15–17). Activation takes place through a two-step mechanism involving first activation by phosphatidylinositol-4,5 bisphosphate (PIP_2) binding at the membrane (18,19). This induces a change in conformation that makes threonine 567 in the C-ERMAD accessible for phosphorylation by Rho-kinase and several PKC isoforms (20–22). Membrane targeting of ezrin is strongly affected by PIP_2 binding. As a consequence, changes in the abundance of PIP_2, due for example to increased hydrolysis by phospholipase C, lead to changes in the amount of membrane-associated ezrin (23). Once bound to PIP_2, the FERM domain mediates lateral interaction with the cytoplasmic tails of transmembrane proteins or scaffolding proteins, such as EBP50-PDZK1 complexes that organize large clusters of submembranous signaling proteins (3). In addition, phosphorylation of threonine 567 in the C-ERMAD

Editor: Cecile Sykes.

CrossMark

induces a transition from inactive ezrin oligomers to active membrane-associated monomers that act as membrane-cortex cross-linkers (16). At the C-terminal, ezrin associates with the cytoskeleton through its F-actin binding domain. Like most proteins, ezrin constantly turns over, associating/dissociating to/from the membrane/cortex and diffusing in the plane of the membrane. In microvilli, photobleaching experiments revealed the presence of complex turnover dynamics that were hypothesized to reflect translocation from the cytoplasm to the membrane, fast diffusion within the membrane, and a stabilized irreversible state due to F-actin binding (24). However, the molecular mechanism underlying this stabilized state and its dependence upon binding to F-actin remain unclear. Despite the fundamental role of ezrin in cortex mechanics and regulation, little is known about its turnover kinetics at the membrane-cortex interface. Yet, these will strongly influence the mechanical properties of linkage between the membrane and the cytoskeleton as well as dictate the spatial accuracy and timescale of signaling through ezrin-associated proteins.

Here, we investigate the molecular origins of ezrin turnover at the membrane-cortex interface using fluorescence recovery after photobleaching (FRAP) experiments together with single molecule imaging. Fitting fluorescence recovery kinetics with an exponential basis of functions revealed that three distinct molecular processes dominated ezrin turnover at different timescales. Separate measurements of the turnover kinetics of the FERM domain and the actin binding domain of ezrin allowed identification of their respective contributions to full-length ezrin turnover. These results were qualitatively and quantitatively confirmed using chemical perturbation, single-molecule imaging, and fluorescence loss after permeabilization experiments.

MATERIALS AND METHODS

Additional information about cell culture, plasmids, transfection, F-actin staining, staining analysis, permeabilization experiments, and chemical treatments is given in the Methods section in the Supporting Material.

FRAP experiments

FRAP experiments were performed using a 1.3 NA 100× oil-immersion objective on a scanning laser confocal microscope (Fluoview FV1000, Olympus, Berlin, Germany). Green fluorescent protein (GFP) was excited at a 488 nm wavelength and light was collected at 525 nm. For live imaging, laser intensities of 5–15% of a 20 mW laser were utilized to obtain a strong signal, and images were acquired at 0.05- to 1-s intervals to minimize loss of fluorescence due to imaging while still sampling fluorescence recovery sufficiently fast to resolve recovery kinetics (25).

In FRAP experiments, a small circular region of interest ($r = 2~\mu$m) centered on a portion of the cell membrane was imaged and a smaller circular bleaching region ($r = 1~\mu$m) was chosen in its center. This choice of imaging and bleaching regions helped minimize acquisition-induced fluorescence loss by not exposing the whole cell to light, and use of confocal microscopy restricted photobleaching to an optical section of thickness 0.6 μm (Fig. S1 in the Supporting Material). Bleaching was performed by scanning the 488 nm beam operating at 100% laser power over the bleach region. In our protocol,

two frames were acquired for normalization of the fluorescence signal, bleaching was effected with one iteration of the laser pulse with a dwell time of 8 μs/pixel and a typical duration of 2 s, and recovery was monitored over 100 frames. To assess fluorescence loss due to imaging, we simultaneously recorded fluorescence from a membranous region separate from the bleached region. In all cases, the rate of imaging-induced fluorescence loss was significantly smaller than the rates of fluorescence recovery, with a characteristic time of $\tau_{\text{fluorescence loss}} \sim 500$ s, one order of magnitude larger than the slowest recovery timescale observed for ezrin. Hence, imaging-induced fluorescence loss did not significantly affect turnover measurements. For each construct, we acquired fluorescence recovery after photobleaching (FRAP) curves from at least 20 individual cells. These were acquired over the course of at least three independent experiments for all constructs except GFP-CT, CT-GFP, GFP-ABD-T567D, and ABD-GFP, for which two independent experiments were performed.

FRAP data analysis

FRAP data analysis was effected as described in Fritzsche et al. (25). As the membrane and the actin cortex are in close apposition (<100 nm (26)), the total fluorescence signal at the membrane-cortex interface results from proteins bound to the actin cortex, the membrane, or both, as well as proteins freely diffusing in the interstice between the cortical actin mesh and the membrane or through the actin mesh (Fig. 1 B). Therefore, FRAP will have contributions from 1) cytosolic diffusion between the membrane and the cortex (cytosolic diffusive recovery); 2) diffusion of membrane-associated proteins in the plane of the membrane (membrane diffusive recovery); and 3) association/dissociation of proteins to/from the cortex or the membrane (reactive recovery) (26,27). Previous reports have measured a diffusion constant of $D \sim 30~\mu\text{m}^2\,\text{s}^{-1}$ for ezrin-GFP in the cytoplasm of epithelial cells (24). Therefore, in our experimental geometry, diffusion of ezrin-GFP should take place on a characteristic timescale of $\tau \sim r^2/4D \sim 10$ ms with $r = 1~\mu$m the radius of the bleach zone, close to the timescale measured for diffusive recovery of GFP in our previous work (25) and several-fold shorter than the characteristic times of the reactions examined in this study ($\tau \geq$ 400 ms). Thus, given the acquisition rate used in our experiments (0.05–1 s/frame), diffusive recovery was complete by the time we acquired the first postbleach frame. Therefore, the fluorescence recovery measured in our experiments was solely due to cortical/membranous fluorescence recovery (comprising the second and third of the contributions listed above, collectively referred to here as cortical recovery). To determine how many first-order molecular processes contributed to turnover, cortical recovery $F(t)$ was fitted with a combination of exponential functions F_i of the form $F_i(t) \sim 1 - \exp(-t/\tau_{\text{d},i})f_i F_0$, where F_0 is the initial fluorescence of the bleached region and i a molecular process participating in recovery. Each function F_i represents the contribution of the molecular process i to the total recovery, with f_i the portion of the total protein population undergoing turnover process i ($\Sigma_i f_i = 1$), and $\tau_{\text{d},i}$ the characteristic dissociation time of process i. The characteristic dissociation time τ_d is linked to the half-time reported in most FRAP experiments: $t_{1/2} = \ln(2)\tau_\text{d}$. The apparent association time $\tau_{\text{a},i}$ can be calculated as $\tau_{\text{a},i} = (\tau_{\text{d},i}/f_i) \times (F_0/F)$ (25). If turnover results from association/dissociation of a protein to/from the cortex, τ_d can also be expressed as an apparent dissociation rate, $\omega_\text{d} = 1/\tau_\text{d}$. One limitation of this analytical approach is that it can only distinguish molecular processes that occur on sufficiently different timescales. If several molecular processes occur at similar timescales, they cannot be distinguished and the apparent rate constant measured reflects an average over all of the molecular processes acting at that timescale. In practice, fluorescence recovery curves $F(t)$ were fitted with an increasing number of exponential functions until three conditions were met: the goodness of fit estimated through r^2 no longer increased; the total change in fluorescence associated with process n was <0.001%; and the sum of squared errors no longer decreased.

Hence, this approach allows determination of the number of molecular processes i that contribute to fluorescence recovery, their characteristic times $\tau_{\text{d},i}$ and the portion f_i of the total protein population that recovers
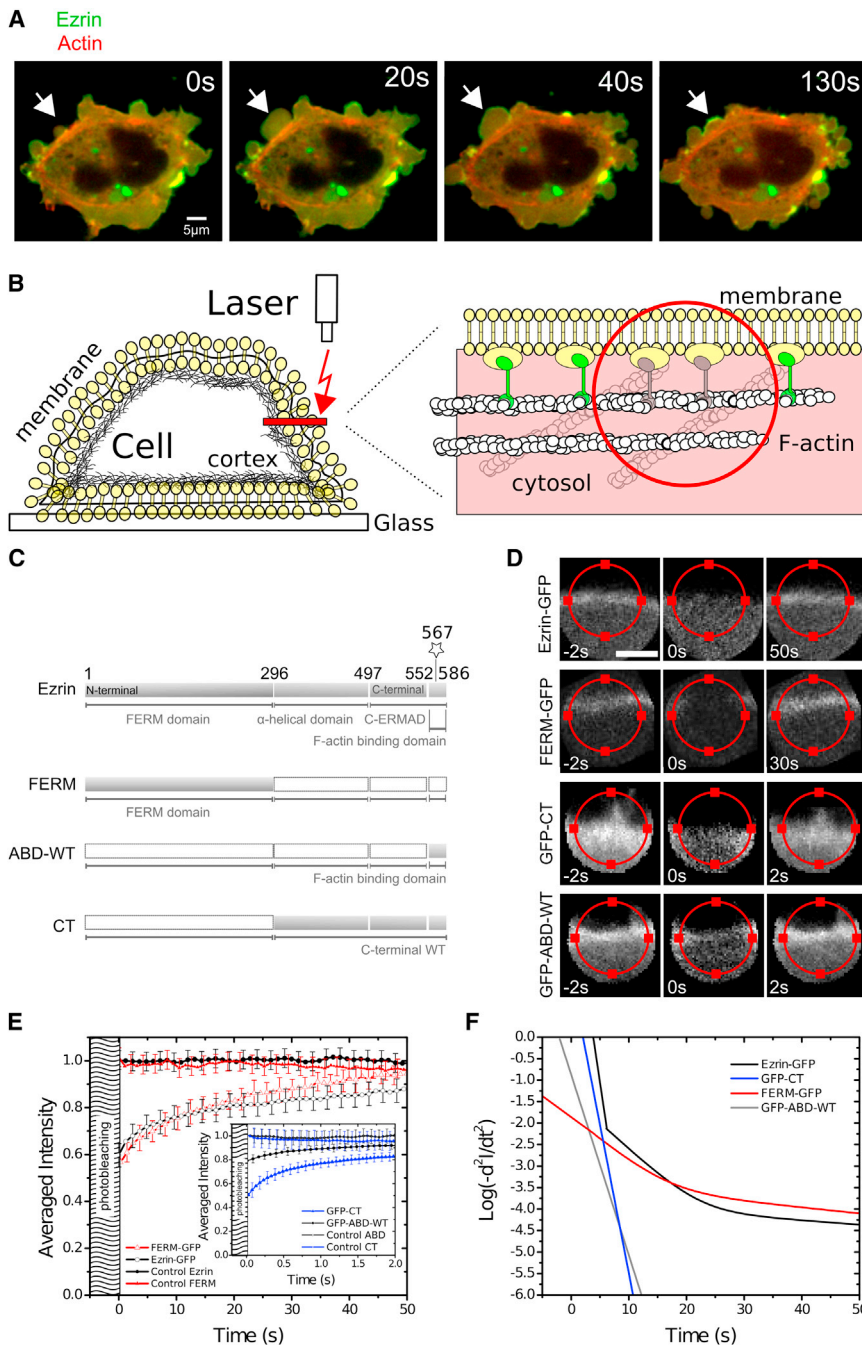
FIGURE 1 Ezrin turnover kinetics at the membrane-cortex interface. (*A*) Time series displaying localization of ezrin (*green*) and actin (*red*) in M2 blebbing melanoma cells. Ezrin strongly localized to the membrane-cortex interface. In growing blebs (*arrow*, $t = 0$ s), ezrin was initially absent from the membrane but appeared toward the end of growth ($t = 20$ s), progressively becoming more enriched ($t = 40$ s). During retraction, it was strongly enriched distal to the actin cortex ($t = 130$ s). (*B*) FRAP experiments were performed in a circular region 1 μm in diameter comprising the cell membrane and the submembranous cortex (*red circle*). Fluorescent membrane-bound proteins are shown in green and bleached ones in gray. After photobleaching, fluorescence in the membrane can recover through diffusion of fluorescent proteins in the cytosol (cytosolic diffusive recovery), diffusion of membrane-associated proteins in the plane of the membrane (membranous diffusive recovery), association/dissociation of fluorescent proteins to the membrane (membrane reactive recovery), or association/dissociation of proteins to the cortex (cortex reactive recovery). (*C*) Schematic representation of the ezrin constructs used in this study. Full-length ezrin consists of a FERM domain, an α-helical domain, and a C-ERMAD domain that contains an F-actin binding domain (ABD). The boundaries of these domains in amino acids are indicated above the graphs. The location of threonine 567 is indicated by a star. (*D*) Consecutive confocal images of FRAP experiments in a region comprising the actin cortex and the cell membrane for cells expressing GFP-tagged full-length ezrin, FERM, CT, and ABD. GFP fluorescence was bleached within the red circle between times $t = -2$ s and $t = 0$ s. Timings for each image are given in seconds. Scale bar, 0.5 μm. (*E*) Fluorescence recovery after photobleaching of ezrin-GFP (averaged over 25 cells) and FERM-GFP (averaged over 22 cells). (*Inset*) Fluorescence recovery of GFP-ABD ($N = 25$ cells) and GFP-CT ($N = 35$ cells) occurred on significantly faster timescales. Control curves show the evolution of fluorescence intensity in a region of the cortex outside of the bleached region. Symbols indicate experimental data points, and for display clarity, only every second data point is shown. Error bars indicate standard deviations, and for clarity, these are only shown for every fourth data point. (*F*) Logarithmic acceleration plots for ezrin-GFP (*black line*), GFP-ABD (*gray line*), GFP-CT (*blue line*), and FERM-GFP (*red line*). In these plots, each linear segment reports on the dominance of one molecular turnover process, with its slope reflecting the apparent reaction rate, $\omega_{d,i} = 1/\tau_{d,i}$. Fit parameters are reported in Tables 1 and S1. To see this figure in color, go online.

through process i. In this analysis, changes in the recovery half-time $t_{1/2}$ may therefore result from changes in the number of processes i participating in recovery, changes in the characteristic times $\tau_{d,i}$ of some or all of the processes, changes in the relative importance f_i of some or all of the turnover processes, or a combination of all of these factors. Therefore, analysis of fluorescence recovery using multiexponential fitting allows for a more precise characterization of turnover and the changes occurring in response to perturbations.

Theoretical derivations and detailed fitting procedures are given in Fritzsche et al. (25).

Single-molecule imaging

Single-molecule imaging was performed using a 1.4 NA 100× oil-immersion objective on an IX-81 microscope (Olympus) equipped with a spinning disk head (CSU22, Yokogawa, Tokyo, Japan) and an iXon EMCCD camera (Andor, Belfast, United Kingdom). Images were acquired with 100% intensity of a 20 mW laser and an 800 ms integration time to obtain a strong fluorescence signal from single fluorophores (27). Images were acquired at 0.5- to 2-s intervals and speckles could be followed for up to 30 frames.

RESULTS

To study the kinetics of ezrin turnover at the membrane-cortex interface, we chose to do our experiments in M2 blebbing melanoma cells, because these cells possess a well-defined contractile actin cortex with few microvilli and ERM proteins have been shown to play a crucial role in linking their membrane to their cortex (1).

Ezrin exhibits complex turnover kinetics at the membrane-cortex interface

In transfected cells, full-length ezrin-GFP localized primarily to the interface between the actin cortex and the plasma membrane, along with a cytoplasmic pool reflecting unbound inactive protein (Fig. 1 A), as previously reported (1). Ezrin was initially absent from growing blebs but was recruited to their membrane before the cessation of growth, and during retraction, a strong enrichment in ezrin was observed distally from the actin cortex (Fig. 1 A) (1). After photobleaching, ezrin fluorescence recovered uniformly throughout the bleaching region (Fig. 1 D) with a half-time of $t_{1/2} = 15.8 \pm 2.0$ s, and recovery was complete within ~60 s ($N = 25$ cells; Fig. 1 E). To determine how many molecular processes participated in ezrin fluorescence recovery at the membrane-cortex interface, we fitted experimental fluorescence recovery curves with an increasing number of exponential functions. This analysis revealed that three exponential functions were necessary to fit the experimental data, suggesting that ezrin turnover at the membrane-cortex interface resulted from three distinct molecular processes, which dominated recovery on different timescales. The identified turnover processes had characteristic times of $\tau_{d,1,ezrin} = 0.4 \pm 0.1$ s, $\tau_{d,2,ezrin} = 3.3 \pm 0.6$ s, and $\tau_{d,3,ezrin} = 50 \pm 25$ s (25 of 25 curves examined; Tables 1 and S1). To visualize these processes graphically, we generated logarithmic plots of the second derivative of F (referred to as logarithmic acceleration plots) that consist of piecewise linear segments with each segment corresponding to a different process and its slope equal to $-1/\tau_{d,i}$ (Fig. 1 F). In addition to the timescales of the molecular pro-

cesses involved in ezrin fluorescence recovery, our analysis enabled us to determine the relative contribution of each turnover process i to total recovery or, equivalently, the portion of total protein undergoing turnover process i (see FRAP data analysis). The first and fastest molecular turnover process accounted for 10% of the total fluorescence recovery ($f_1 = 0.1$), the second for 60% ($f_2 = 0.6$), and the third for 30% ($f_3 = 0.3$). The timescales of processes 2 and 3 were qualitatively similar to those reported for ezrin in microvilli (24), but process 1 was not identified in previous reports.

Molecular dissection of ezrin turnover at the membrane-cortex interface

Based on the known molecular functions of ezrin domains (3), ezrin fluorescence recovery at the membrane-cortex interface might stem from 1) association of ezrin proteins to the membrane via their FERM domain; 2) association of ezrin proteins to the actin cortex via their actin-binding domain (ABD); or 3) diffusion of membrane-associated ezrin into the bleached zone. To gain insight into the molecular origin of full-length ezrin turnover processes, we characterized the turnover kinetics of the FERM and ABD domains of ezrin alone (Fig. 1 C). Indeed, given the well-characterized functions of the FERM and ABD domains (3,22), we reasoned that the fluorescence recovery kinetics of these domains should reflect some of the molecular processes identified in full-length ezrin. As overexpression of ezrin's functional domains may potentially perturb the function of endogenous proteins (e.g., overexpression of FERM perturbs membrane-cortex attachment and bleb retraction (1)), we carried out our FRAP experiments in cells expressing moderate levels of fluorescently tagged protein domains and visually verified that cellular phenotype appeared normal based on cell morphology, bleb abundance, and bleb dynamics.

FERM-GFP localized exclusively to the cell membrane and was present at all stages of the bleb life cycle (Movie S1), consistent with previous reports (1). As blebs are initially devoid of an actin cortex during growth (Fig. 1 A,

TABLE 1   Characteristic dissociation times for the molecular processes participating in the turnover of each construct

Protein	$\tau_{d,1}$ (s)	p-Value	f_1	$\tau_{d,2}$ (s)	p-Value	f_2	$\tau_{d,3}$ (s)	p-Value	f_3	N
Ezrin-GFP	0.4 ± 0.1	—	0.1	3.3 ± 0.5	—	0.6	50 ± 25	—	0.3	25
FERM-GFP	—	—	—	4.0 ± 0.5	<0.01	0.65	50 ± 25	0.98	0.35	22
GFP-CT	0.4 ± 0.1	0.96	1.0	—	—	—	—	—	—	35
CT-GFP	0.4 ± 0.1	0.93	1.0	—	—	—	—	—	—	21
GFP-ABD (WT)	1.02 ± 0.1	<0.01	1.0	—	—	—	—	—	—	25
ABD-GFP	0.95 ± 0.1	<0.01	1.0	—	—	—	—	—	—	20
GFP-ABD-T567D	1.0 ± 0.1	<0.01	1.0	—	—	—	—	—	—	25
Ezrin-T567D-GFP	0.7 ± 0.1	<0.01	0.6	5.0 ± 1.3	<0.01	0.1	100 ± 50	<0.01	0.3	24
Ezrin-GFP + lat B	—	—	—	2.8 ± 0.8	0.84	0.68	26 ± 5	<0.01	0.32	25

The statistical significance of differences in characteristic dissociation times between full-length protein and different functional domains or chemical perturbations is given in terms of the corresponding p values, with the abundances, f_i, of each molecular turnover process. GFP, green fluorescent protein; WT, wild-type.

red (1,28)), this indicated that FERM localization did not depend on the presence of a submembranous F-actin cortex, as expected for a domain with no actin binding (1). After photobleaching, FERM fluorescence recovered uniformly throughout the bleached region with half-time $t_{1/2} = 18.6 \pm 2$ s ($N = 22$ cells; Fig. 1, *D* and *E*), and recovery was complete in ~60 s. Multiexponential fitting revealed that only two molecular processes participated in turnover of FERM (22 of 22 curves examined; Tables 1 and S1 and Fig. 1 *F*). The characteristic time of the first FERM turnover process was comparable to that of the second turnover process of full-length ezrin, but significantly larger ($\tau_{d,1,FERM} = 4.0 \pm 0.5$ s vs. $\tau_{d,2,ezrin} = 3.3 \pm 0.6$ s, $p < 0.01$), whereas the second FERM turnover process had a characteristic time identical to that of the third turnover process of full-length ezrin ($\tau_{d,2,FERM} = 50 \pm 25$ s vs. $\tau_{d,3,ezrin} = 50 \pm 25$ s, $p = 0.98$; Fig. 1 *F* and Tables 1 and S1).

ABD tagged with GFP at its N-terminus (GFP-ABD; Fig. 1, *C* and *D*) localized to the cell cortex and was absent from bleb membranes during expansion before being recruited once expansion slowed, consistent with its known F-actin binding properties and the transient absence of F-actin from bleb membranes during expansion (1,28). After photobleaching, ABD fluorescence recovered uniformly throughout the bleached region with a half-time $t_{1/2} = 0.7 \pm 0.1$ s ($N = 25$ cells; Fig. 1 *D*), and recovery was complete within ~2 s (Fig. 1 *E*), a turnover far more rapid than those seen for full-length ezrin or FERM. As expected from its function and short length (34 amino acids), turnover of ABD could be fitted by a single exponential with characteristic time $\tau_{d,GFP-ABD} = 1.0 \pm 0.1$ s ($N = 25$ cells; Fig. 1 *F*), signifying that only binding to F-actin governed its turnover. This characteristic time was close to, but significantly longer than, that of the first turnover process detected for full-length ezrin ($\tau_{d,1,ezrin} = 0.4 \pm 0.1$ s, $p < 0.01$). Similar kinetics and localization were measured for ABD tagged with GFP at its C-terminus (ABD-GFP, $\tau_{d,ABD-GFP} = 0.95 \pm 0.05$ s, $N = 20$ cells, $p = 0.94$ when compared to GFP-ABD; Tables 1 and S1, and Movie S2). To examine whether the slower dissociation rate observed for the first turnover process in full-length ezrin reflected the dynamics of the active ABD, we measured the turnover kinetics of the ABD harboring a phosphomimetic mutation on threonine 567 (GFP-ABD-T567D). ABD-T567D had a characteristic dissociation time, $\tau_{d,ABD-T567D} = 1.0 \pm 0.1$ s ($N = 25$ cells), identical to that of wild-type ABD. As the large size of the GFP tag compared to the ABD (238 amino acids (aa) for GFP compared to 34 aa for ABD) might interfere with F-actin binding, we repeated our experiments with constructs encoding the C-terminal portion of ezrin (Fig. 1 *C*), reasoning that its longer length (290 aa) should prevent disruption of F-actin binding by GFP tagging. The C-terminal (CT) domain tagged at its N-terminus (GFP-CT) had a localization identical to that of the ABD (Movie S3 and Fig. 1 *D*), and its turnover could be fitted with a single expo-

nential with a characteristic time of $\tau_{d,CT} = 0.4 \pm 0.1$ s ($N = 35$ cells; Fig. 1 *F*). This characteristic dissociation time was identical to that of full-length ezrin ($p = 0.96$) but faster than that of ABD, suggesting that ABD binding to F-actin is more stable than binding of CT or full-length ezrin. Identical kinetics and localization were measured for CT tagged with GFP at its C-terminus (CT-GFP, $\tau_{d,CT-GFP} = 0.4 \pm 0.1$ s, $N = 21$ cells, $p = 0.98$ when compared to GFP-CT; Tables 1 and S1 and Movie S4). Together, these data suggested that ezrin associates and dissociates from cortical F-actin on timescales of <1 s.

Ezrin dissociates rapidly from the F-actin cortex

The short timescale of ezrin attachment to and detachment from the F-actin cortex was surprising, since previous work has hypothesized that ezrin association with F-actin leads to stabilized states with turnover times >60 s (24). Therefore, we sought to confirm our results by measuring the association/dissociation of full-length ezrin to/from the actin cortex using alternative methods. Thus, we monitored ezrin fluorescence after membrane removal by Triton-X100, reasoning that only ezrin bound to F-actin would remain at the cell cortex and therefore that decay in fluorescence would only result from dissociation of ezrin from F-actin.

First, we verified that after membrane removal cells still retained substantial cortical F-actin. In our experiments, we treated cells stably expressing ezrin-mRFP with Triton-X100 for 100 s before fixing them and staining them with Alexa488-labeled phalloidin to visualize their actin cytoskeleton. This revealed that despite the removal of the plasma membrane, cells still retained an actin cortex morphologically indistinguishable from the cortex of non-permeabilized cells (Fig. 2 *A*, *green*), and that cells also retained some cortical ezrin (Fig. 2 *A*, *red*). To quantify cortical F-actin loss due to membrane removal, we compared cortical fluorescence intensity of phalloidin staining in cells fixed before membrane removal to that of cells fixed 100 s after membrane removal (Fig. 2 *B*). Membrane removal resulted in a $27 \pm 19\%$ decrease in cortical F-actin fluorescence ($p < 0.01$ compared to control, $N = 30$ cells examined for each condition). Together, these data showed that cells retained a well-defined actin cortex even 100 s after membrane removal.

Next, we monitored the dynamics of ezrin fluorescence change after membrane removal. Before permeabilization, ezrin fluorescence was maximal at the membrane-cortex interface. After permeabilization, a clear cortical fluorescence signal remained (Fig. 2 *C* and Movie S5), and this decayed rapidly, losing ~50% of its intensity in 2.1 ± 1 s ($N = 28$ measurements from 18 cells; Fig. 2 *D*). One hundred seconds after membrane removal, ezrin cortical fluorescence intensity had decreased by $76 \pm 10\%$ (Fig. 2 *D*) compared to a decrease of $27 \pm 19\%$ for F-actin (Fig. 2 *B*). This implied
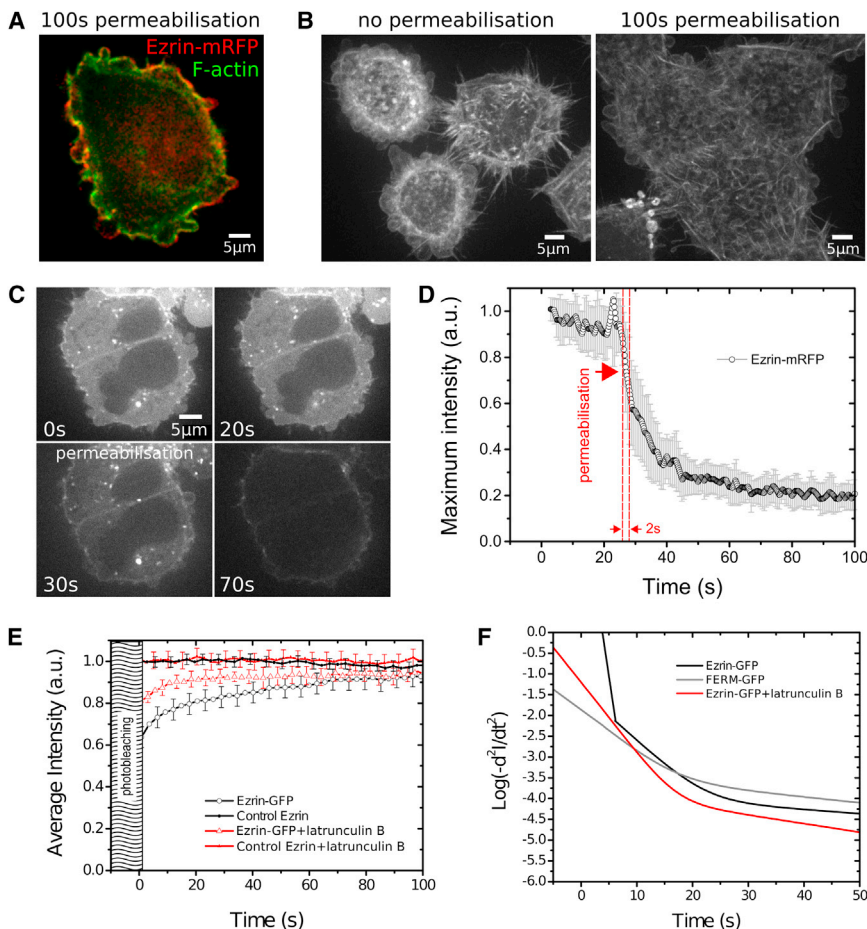
FIGURE 2 The first fast turnover process is due to F-actin binding. (A) Representative localization of F-actin and ezrin-mRFP after 100 s permeabilization. F-actin localization was visualized using Alexa488-Phalloidin staining. (B) Representative localization of F-actin in cells fixed before or 100 s after membrane removal. F-actin localization was visualized using Alexa488-Phalloidin staining, and both images were acquired with the same acquisition settings. The intensity scale was kept identical for both images to allow visual comparison of F-actin fluorescence intensities before and after membrane removal. (C) Dissociation of ezrin from F-actin can be measured by removal of the membrane by detergent extraction in cells expressing ezrin-mRFP. After 25 frames acquired at 1 s intervals, the membrane was removed and only ezrin-mRFP bound to F-actin remained. Fluorescence decay over time was due to dissociation of the ezrin ABD from the cortex. The intensity scale was kept constant for all images to allow visual comparison between time points. (D) Temporal evolution of ezrin fluorescence at the cortex. The red arrow indicates the timing of permeabilization and the dotted lines indicate an interval of 2 s during which ~50% of fluorescence is lost. (E) Fluorescence recovery after photobleaching of ezrin-GFP in control cells (averaged over 25 cells; *black lines*) and cells treated with latrunculin B to depolymerize the actin cytoskeleton (averaged over 25 cells; *red lines*). Control curves show the evolution of fluorescence intensity in a region of the cortex outside of the bleached region. Symbols indicate experimental data points, and for display clarity, only every second data point was displayed. Error bars indicate standard deviations, and for clarity, these are only shown for every fourth data point. (F) Logarithmic acceleration plots for ezrin-GFP in control cells (*black line*), cells treated with latrunculin B (*red line*), and the FERM domain of ezrin (*gray line*). In these plots, each linear segment reports on the dominance of one molecular turnover process, with its slope reflecting the apparent reaction rate, $\omega_{d,i} = 1/\tau_{d,i}$. Fit parameters are reported in Tables 1 and S1. To see this figure in color, go online.

that the decrease in cortical ezrin could not be ascribed to an equivalent loss in cortical F-actin. Decay of cortical ezrin fluorescence after membrane removal was comparable to, but significantly slower than, the timescale of GFP-ABD or GFP-CT dissociation from the cortex measured by FRAP ($\tau_{d,GFP-ABD} = 1.0 \pm 0.1$ s and $\tau_{d,GFP-CT} = 0.4 \pm 0.1$ s, respectively), perhaps because removal of the cell membrane by Triton-X100 was not instantaneous. Nonetheless, the measured half-time of ezrin fluorescence decay was 30-fold shorter than that hypothesized to be associated with ezrin binding to F-actin in microvilli (24). Together with our FRAP data, this suggested that the first fast turnover process of full-length ezrin resulted from the association/dissociation kinetics of its ABD to/from cortical F-actin.

To obtain independent confirmation of these results, we examined ezrin turnover in cells whose actin cytoskeleton had been depolymerized using the G-actin sequesterer latrunculin B. Previous work has shown that ezrin localization to the cortex is independent of F-actin (1), and we reasoned therefore that upon F-actin depolymerization, ezrin turnover should reflect the kinetics of its membrane association only. In cells treated with 750 nM latrunculin B for 20 min, after photobleaching, ezrin fluorescence recovered uniformly throughout the bleached region with half-time $t_{1/2} = 8.5 \pm 1$ s ($N = 25$ cells; Fig. 2 E), and recovery was complete in ~60 s. Multiexponential fitting revealed that only two molecular processes participated in turnover (25 of 25 curves examined, Tables 1 and S1 and Fig. 2 F). The characteristic time of the first turnover process of ezrin in cells treated with latrunculin B was not significantly different from that of the second turnover process of ezrin in control cells ($\tau_{d,1,ezrin+latrunculin} = 2.8 \pm 0.8$ s vs. $\tau_{d,2,ezrin} = 3.3 \pm 0.6$ s, $p = 0.68$); whereas the second turnover process had a characteristic time significantly shorter than ezrin's third turnover process in control cells ($\tau_{d,2,ezrin+latrunculin} = 25 \pm 5$ s vs. $\tau_{d,3,ezrin} = 50 \pm 25$ s, $p < 0.01$; Fig. 2 F and Tables 1 and S1). The absence of ezrin's first fast turnover process in cells treated with latrunculin B again suggested that that process reflected association of ezrin to F-actin. Together, these data confirmed that ezrin's first fast turnover process was due to binding

to cortical F-actin via ezrin's ABD, and that dissociation occurred on timescales of <1 s.

FERM turnover results from membrane binding and diffusion in the plane of the membrane

Next, we investigated the origin of FERM turnover using single-molecule imaging. In single-molecule imaging, contrast formation results from the low expression levels of GFP-tagged proteins and the very long image acquisition times (700 ms) employed: proteins that diffuse in the cytosol contribute to background signal, whereas proteins that stay immobile during the time frame of acquisition (either because they are bound to an immobile structure or because they diffuse very slowly) appear as diffraction-limited

fluorescent speckles (29). Between these extremes, membranous proteins that diffuse with characteristic times comparable to the acquisition time should generate streaks of fluorescence that reflect their mean-square displacement and hence their diffusion constant, D (mean-square displacement, $\sim 2Dt$).

First, to calibrate our imaging protocol, we imaged actin speckles, reasoning that GFP-actin molecules incorporated into F-actin in the cortex should give rise to sharp speckles, as they do when incorporated into actin filaments in the lamellipodium (29). As expected, single actin molecules appeared as diffraction-limited spots with lifetimes on the order of ~ 5.4 s (Fig. 3 A and Movie S6). When time projections of single-molecule imaging movies were generated, long streaks of fluorescence that reflected the trajectory of
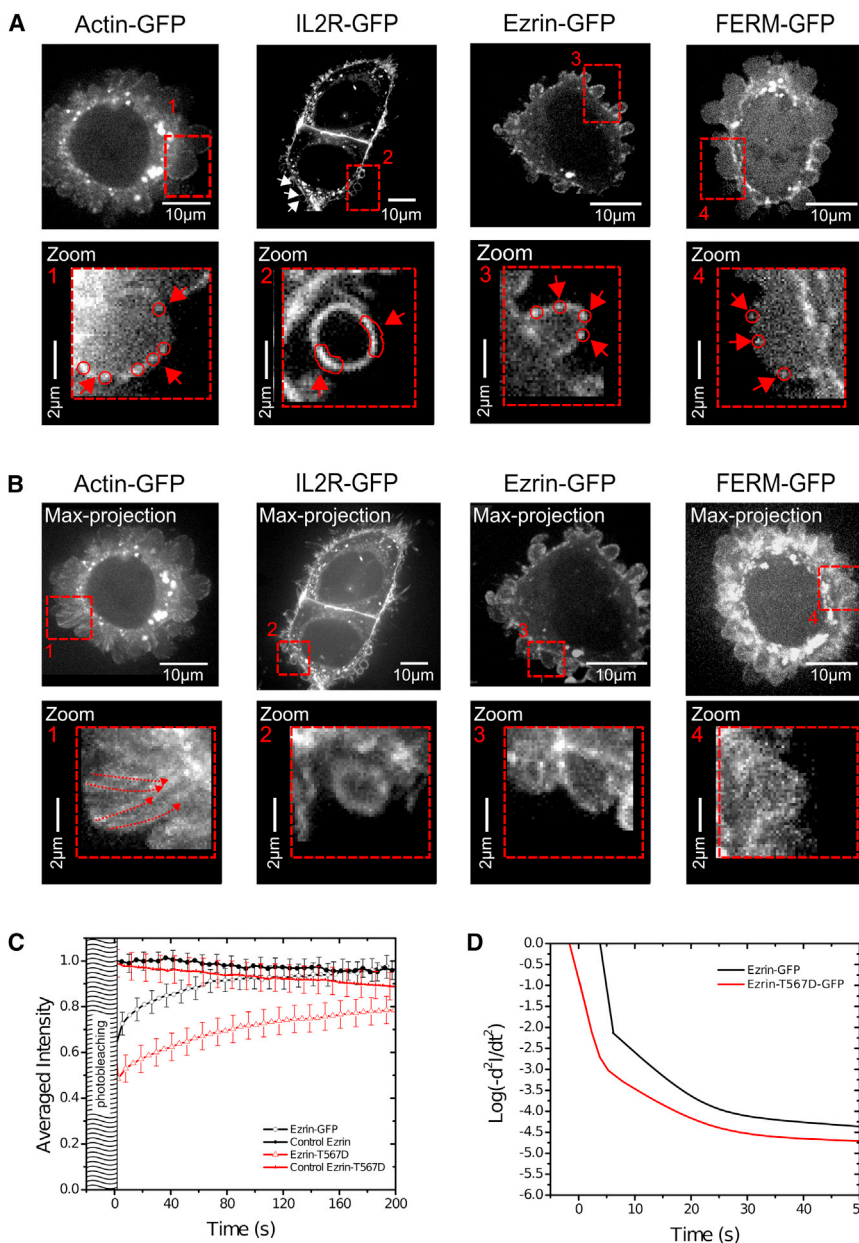

FIGURE 3 Molecular turnover processes identified by single-molecule speckle experiments and dynamics of phosphomimetic ezrin-T567D. (*A*) Single-molecule imaging for cells expressing ΔCMV-GFP-actin, ΔCMV-IL2R-GFP, ΔCMV-ezrin-mRFP, and ΔCMV-FERM-mRFP (*upper row*). The lower row shows a zoom of the boxed region in the upper row. Arrows indicate the location of single-molecule speckles. Actin, ezrin, and ERM molecules appeared as well defined speckles (*red circles*), whereas IL2R appeared as ~ 1 μm long streaks (outlined in red). (*B*) Trajectories of single molecules visualized in time-projection images. Thirty time points were projected onto one single image representing 60 s. Clear trajectories can be observed for actin molecules but not for IL2R, ezrin, or FERM. Arrows indicate trajectories. The lower row shows a zoom of the boxed region in the upper row. (*C*) Fluorescence recovery after photobleaching of ezrin-GFP (averaged over 25 cells; *black line*) and ezrin-T567D-GFP (averaged over 24 cells; *red line*). Control curves show the evolution of fluorescence intensity in a region of the cortex outside of the bleached region. Symbols indicate experimental data points, and for clarity only every second data point is displayed. Error bars indicate standard deviations, and for clarity these are only shown for every fourth data point. (*D*) Logarithmic acceleration plots for ezrin-GFP (*black line*) and ezrin-T567D-GFP (*red line*). In these plots, each linear segment reports on the dominance of one molecular turnover process with its slope reflecting the apparent reaction rate, $\omega_{d,i} = 1/\tau_{d,i}$. Fit parameters are reported in Tables 1 and S1. To see this figure in color, go online.

actin speckles incorporated into the actin cortex could be observed in retracting blebs (Fig. 3 B, *red arrows*). Next, to qualitatively characterize the aspect of speckles of membranous proteins, we generated a construct encoding the ectodomain and transmembrane domain of the interleukin 2 receptor (IL2R) tagged with GFP. This construct did not possess a cytoplasmic domain and therefore could not associate with binding partners within the cell. When imaged using our single-molecule acquisition protocol, IL2R proteins appeared as streaks ~1 μm long that rapidly moved in the plane of the membrane over time (Fig. 3 A and Movie S7). The length of fluorescence streaks indicated a diffusion constant, $D_{IL2R} \sim x^2/t \sim 1$ μm^2/s (with x the streak length and t the acquisition time, ~1 s), typical for membrane bound proteins (30,31) (Fig. 3 A). In contrast to actin speckles, time-projection images did not reveal well-defined trajectories for IL2R in retracting blebs, consistent with the rapid displacement of streaks in the plane of the membrane over time (Fig. 3 B).

Next, we examined the aspect and lifetimes of full-length ezrin and FERM speckles. Both proteins appeared as sharp, well-defined fluorescence speckles that persisted for several seconds before disappearing (Fig. 3, A and B, and Movies S8 and S9). The average lifetime of FERM speckles was $\tau_{FERM\ speckles} = 3.2 \pm 3$ s ($N = 83$ speckles), close to the characteristic timescale of the first turnover process for FERM, $\tau_{1,FERM} = 3.3$ s, and the second turnover process for ezrin, $\tau_{d,2,ezrin} = 3.3 \pm 0.6$ s, identified by FRAP. This suggested that the first turnover process of FERM resulted from association/dissociation of FERM from its membrane binding partners. This view was supported by FRAP data and time-projection images. Indeed, if we assume that a FRAP turnover process results from diffusion in the plane of the membrane, its diffusion constant, D, can be calculated as $D \sim r^2/4\tau$, where r is the radius of the bleach zone and τ the characteristic time (32,33). For FERM, this yields $D_{FERM,1} \sim 0.1$ μm^2/s and $D_{FERM,2} \sim 0.01$ μm^2/s. Hence, if the first turnover process of FERM was due to diffusion and the second to association/dissociation, FERM speckles would have very long lifetimes and diffuse slowly. Therefore, in time-projection images of retracting blebs, we would expect to observe long speckle trajectories similar to those obtained for actin, something that was not supported by our experimental data (Fig. 3 B). Hence, we concluded that the first turnover process of FERM resulted from association/dissociation from its membrane binding partners and the second from slow diffusion in the membrane.

Activated ezrin T567D stabilizes ezrin binding to the actin cortex

Many studies of ezrin have utilized a constitutively active phosphomimetic form of ezrin (ezrin-T567D) to explore the effects of ezrin overactivation. Biochemical evidence has shown that this point mutation leads to a transition

from dormant oligomers to active membrane-associated monomers that cross-link the membrane to the actin cortex (16,17). Therefore, we analyzed turnover kinetics of ezrin-T567D mutants to characterize the kinetics of active ezrin monomers at the cortex.

When transfected into cells, ezrin-T567D-GFP displayed a strong cortical localization with a markedly decreased cytoplasmic pool compared to wild-type ezrin, consistent with results of previous work in blebbing melanoma cells (1). Similar to wild-type ezrin, ezrin-T567D fluorescence recovered uniformly throughout the bleach region with a half-time of $t_{1/2} = 34 \pm 3$ s, significantly longer than that for wild-type ezrin ($N = 24$ cells, $p < 0.01$). Analysis of its fluorescence recovery revealed a significant increase in the characteristic times of all turnover processes ($\tau_{d,1,T567D} = 0.7 \pm 0.1$ s, $\tau_{d,2,T567D} = 5.0 \pm 1$ s, and $\tau_{d,3,T567D} = 100 \pm 50$ s, $p < 0.01$ compared to wild-type ezrin for all characteristic times; Fig. 3, C and D, and Tables 1 and S1). The increase in the characteristic time of actin binding $\tau_{d,1}$ is consistent with constitutive activation resulting from the T567D mutation, with the shorter characteristic dissociation time observed for the ABD that binds F-actin in an unregulated manner, and with the greater association to the cytoskeleton revealed in biochemical assays (16). Surprisingly, the fraction of ezrin-T567D bound to F-actin was significantly larger than for wild-type ezrin ($f_{1,T567D} = 0.6$ and $f_{1,ezrin} = 0.1$, $p < 0.01$; Tables 1 and S1), whereas the total fraction of membrane-bound ezrin was decreased ($f_{2,T567D} + f_{3,T567D} = 0.4$ and $f_{2,ezrin-wt} + f_{3,ezrin-wt} = 0.9$, $p < 0.01$; Tables 1 and S1). Thus, the slower overall turnover kinetics of phosphomimetic ezrin T567D were due to differences in the fraction of protein engaged in each turnover process, as well as longer characteristic times for each of the individual processes.

DISCUSSION

Together, our data show that turnover of ezrin at the membrane-cortex interface results from three separate molecular processes. The timescales of turnover processes 2 (due to ezrin association with the membrane via its FERM domain) and 3 (due to diffusion of membrane-associated ezrin within the plane of the membrane) were in qualitative agreement with the timescales reported in microvilli, whereas process 1 (due to binding of ezrin to F-actin) was not previously identified (24). This may be because ezrin turnover in microvilli differs from turnover in the cortex, or because of differences in cell type. Molecular dissection and single-molecule imaging allowed identification of the molecular origin of each turnover process. The most rapid turnover process stemmed from ezrin proteins bound only to F-actin via their ABD and it accounted for only 10% of total ezrin at the membrane-cortex interface. Interestingly, the characteristic dissociation time for ezrin ABD from F-actin was approximately threefold shorter than that for α-actinin ABD (25), suggesting that structural differences result in

less stable binding or that they bind different types of cortical actin filaments (34). The second and third turnover processes of full-length ezrin reflected interaction with the membrane through the FERM domain. Quantitative and qualitative analysis of single-molecule imaging data identified the third and slowest turnover process as due to diffusion of membrane-associated ezrin, consistent with its known interaction with submembranous scaffolding domains composed of proteins such as EBP-50, PDZK1, and CFTR (3). Previous work has shown that these membrane-associated protein complexes are nearly immobile due to stabilization through F-actin binding via ezrin (35). Together with the very short characteristic time of actin binding, this suggests that many ezrin proteins must be present in each membrane-associated protein complex to ensure constant and stable anchoring to the actin cortex. Consistent with this hypothesis, depolymerization of F-actin with latrunculin B resulted in faster diffusion of ezrin in the plane of the membrane. The turnover process that we identified as due to diffusion of membrane-associated ezrin was previously interpreted as a slow release from F-actin binding (24). However, its presence in the turnover of FERM, which cannot bind actin, argues against such an interpretation. Furthermore, our fluorescence loss after permeabilization experiments independently showed that the characteristic time of ezrin dissociation from F-actin was significantly shorter than the 60 s hypothesized in previous work (24). Finally, measurement of FERM speckle lifetime showed that the second turnover process reflected association/dissociation of the FERM domain to/from the membrane and accounted for the majority of ezrin proteins.
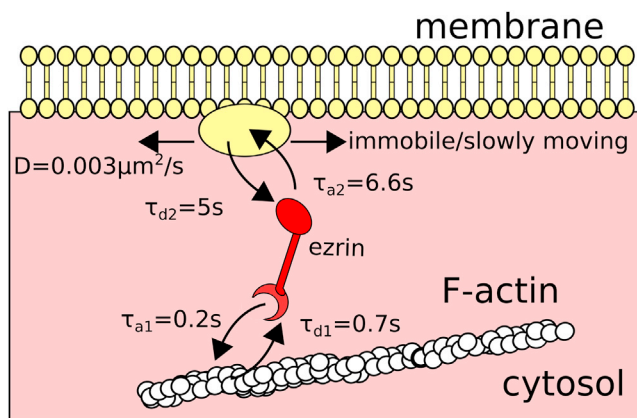
Ezrin can associate with the membrane in either a closed inactive configuration that forms oligomers or in an active open configuration that is monomeric (15,16). Comparison of the turnover kinetics of wild-type ezrin with those of ezrin-T567D offers some insight into the relative importance and turnover kinetics of inactive ezrin oligomers at the membrane. Indeed, biochemical evidence has shown that ezrin-T567D is overwhelmingly monomeric (16). Assuming that the turnover kinetics of ezrin-T567D reflect those of active monomeric wild-type ezrin, and that the distribution of ezrin-T567D across the three molecular processes participating in turnover is representative of the fraction of active monomeric ezrin, we can estimate the fraction wild-type ezrin that is active at the cell membrane. Our experiments revealed that wild-type ezrin distributed into $f_{\text{F-actin binding, wt}} = 10\%$ associating with F-actin, $f_{\text{memb binding, wt}} = 60\%$ associating with the membrane through the FERM domain, and $f_{\text{memb diff, wt}} = 30\%$ membrane-associated and diffusing in the plane of the membrane (Table 1). In contrast, constitutively active ezrin T567D distributed as (Table 1) $f_{\text{F-actin binding, T567D}} = 60\%$, $f_{\text{memb binding, T567D}} = 10\%$, and $f_{\text{memb diff, T567D}} = 30\%$. As ezrin can only bind F-actin when fully activated, we can assume that at least $f_{\text{F-actin binding, wt}} = 10\%$ of wild-type ezrin is active. This allows us to deduce what percentage of active ezrin is present in the membrane-associated fractions based on the distribution of ezrin-T567D. By proportionality, we find that the percentage of active wild-type ezrin binding to the membrane is $(f_{\text{F-actin binding, wt}}/f_{\text{F-actin binding, T567D}}) \times f_{\text{memb binding, T567D}} = 1.6\%$ and the percentage of membrane-associated active wild-type ezrin diffusing in the membrane is $(f_{\text{F-actin binding, wt}}/f_{\text{F-actin binding, T567D}}) \times f_{\text{memb diff, T567D}} = 4.8\%$. This implies that the membrane-associated fractions of wild-type ezrin ($f_{\text{memb diff}}$ and $f_{\text{memb binding}}$) are formed predominantly of inactive oligomers, signifying that the kinetics of the membrane-associated fractions of wild-type ezrin primarily reflect the kinetics of inactive oligomeric forms of ezrin. In addition, comparison of the characteristic dissociation times of ezrin T567D and wild-type ezrin (Table 1) suggest that active ezrin monomers bind more strongly to the membrane and diffuse less rapidly in the plane of the membrane than inactive oligomers. Overall, our results indicate that the majority of membrane-bound wild-type ezrin is composed of dormant oligomers, consistent with previous results obtained by fluorescence resonance energy transfer assays in gastric parietal cells (17). As most of the reported cross-linking or signaling functions of ezrin necessitate activation (3), this suggests that cells possess a large pool of ezrin proteins that can be rapidly mobilized, perhaps through inactivation of threonine 567 dephosphorylation pathways, as proposed by Zhu and colleagues (36).

Surprisingly, no separate timescale was associated with ezrin bound either to the membrane or to F-actin. This may be because the majority of membrane-associated wild-type ezrin is present in the form of inactive oligomers (see above, as well as Gautreau et al. (16) and Zhu et al. (17)) and dominates recovery or because ezrin's actin-binding kinetics are so much faster than its membrane-binding kinetics that F-actin binding only marginally stabilizes ezrin localization to the membrane-cortex interface. Using reasoning similar to that outlined above, we can estimate what fraction of total protein is bound both to the membrane and the cortex. Assuming that active ezrin behaves as ezrin T567D, it partitions into $f_{\text{F-actin binding,T567D}} = 60\%$ bound to the F-actin cortex only and $f_{\text{memb,T567D}} = f_{\text{memb diff,T567D}} + f_{\text{memb binding,T567D}} = 40\%$ bound to the membrane. Proteins bound to the membrane also potentially interact with the F-actin cortex through their actin-binding domain. An estimate of the fraction of ezrin T567D bound to both the F-actin cortex and the membrane is $f_{\text{cross-linking,T567D}} = f_{\text{F-actin binding,T567D}} \times f_{\text{memb,T567D}} = 24\%$. In a similar way, based on the estimates of active membrane-bound wild-type ezrin obtained above ($f_{\text{memb,wt}} = f_{\text{memb diff,wt}} + f_{\text{memb binding,wt}} = 6.4\%$), we can estimate the fraction of wild-type ezrin that is active and bound both to the F-actin cortex and the membrane as $f_{\text{cross-linking,wt}} = f_{\text{F-actin binding,T567D}} \times f_{\text{memb,wt}} = 3.9\%$. Previous work has shown that overexpression of constitutively active ezrin T567D leads to a change in cellular phenotype where

blebbing is severely inhibited (3). In light of the results presented here, this change can now be understood as due to an approximately sixfold increase in the fraction of ezrin protein bound to both the membrane and the F-actin cortex, leading to a strong increase in membrane-cortex adhesion energy. In addition, our experimental data allow us to gain insight into how ezrin cross-links the membrane to the cortex. It is often assumed that ezrin localization to the membrane is stabilized by F-actin binding: when ezrin proteins bound to both F-actin and the membrane lose their attachment to the membrane, they remain at the membrane-cortex interface thanks to their F-actin binding domain. Such a conceptual picture is only true if the average duration of ezrin binding to F-actin is longer than the average time it takes ezrin to associate with the membrane or, equivalently, if the characteristic dissociation time of active ezrin from F-actin ($\tau_{d,1}$ for ezrin T567D) is longer than the characteristic association time of active ezrin to the membrane ($\tau_{a,2}$ for ezrin T567D). Conversely, if $\tau_{a,2} > \tau_{d,1}$, ezrin will detach from F-actin before it can reassociate with the membrane. Our measurements show that $\tau_{d,1} = 0.7 \pm 0.1$ s $< \tau_{a,2} = 6.6 \pm 1.3$ s (Tables 1 and S2). Hence, F-actin binding does not strongly stabilize the presence of active ezrin at the membrane-cortex interface, and after detachment from the membrane, active ezrin primarily diffuses away into the cytosol.

Based on these data, we propose the following conceptual model for ezrin function at the membrane-cortex interface (Fig. 4 and Tables 1, S1, and S2). After association with PIP$_2$ at the membrane and phosphorylation, ezrin binds to the F-actin cortex through an interaction that is highly labile

compared to its membrane binding. Because many ezrin proteins are present, this provides a mechanically stable but highly dynamic link between the membrane and the cortex. From a mechanical point of view, tethering of the membrane to the cortex gives rise to an effective friction between the membrane and the cortex, which can be measured through dynamic tether extraction experiments (37,38). Our results suggest that the rapid kinetics of association/dissociation of ezrin to/from the cortex ensure strong membrane-cortex adhesion energy together with low friction between the membrane and the cortex. Biologically, modulation of the abundance of PIP$_2$ at the cell membrane would offer an efficient way of changing membrane-cortex adhesion energy. Consistent with this, ERM proteins are displaced from the membrane by phospholipase-C-mediated PIP$_2$ hydrolysis to allow cytoskeletal remodeling after chemokine stimulation (23). This may also explain the higher abundance of membrane-associated ezrin in microvilli (24), which necessitate a strong stable attachment between the membrane and the microvillus core, compared to blebs, where the cortex undergoes rapid shape change during retraction and may therefore need more dynamic attachments (39). Hence, the very rapid kinetics of F-actin association/dissociation may ensure that the membrane can exactly conform to cortical shape and provide low-friction tethering that does not impede cell shape change. Conversely, the immobility of the membrane domains to which ezrin associates relative to the actin cortex signifies that signals emanating from these membrane-associated protein complexes may be able to locally modulate cortical organization and contractility on a scale of less than a micron. Given the importance of ERM proteins in cell division (13,14), such kinetics may enable the complex spatiotemporal coordination of cortical actin mechanics necessary to drive cell morphogenesis, and therefore, it will be interesting to determine whether and how ERM protein turnover kinetics vary during cytokinesis.

SUPPORTING MATERIAL

FIGURE 4 Ezrin dynamics at the membrane/cortex interface. A schematic of the three molecular processes underlying the dynamics of active ezrin at the membrane/cortex interface is shown. Active ezrin associates/dissociates from its membrane-binding partners (*yellow oval*) with characteristic times of $\tau_{a,membrane} \sim 6.6$ s and $\tau_{d,membrane} \sim 5.0$ s (Tables 1 and S2). Although it is membrane-bound, it can undergo slow diffusion within the plane of the membrane with a diffusion constant of $D_{membrane} \sim 0.003$ μm^2/s. At its C terminus, ezrin associates/dissociates from the actin cortex with characteristic times of $\tau_{a,cortex} \sim 0.2$ s and $\tau_{d,cortex} \sim 0.7$ s (Tables 1 and S2). To see this figure in color, go online.

REFERENCES

1. Charras, G. T., C. K. Hu, …, T. J. Mitchison. 2006. Reassembly of contractile actin cortex in cell blebs. *J. Cell Biol.* 175:477–490.

2. Ivetic, A., and A. J. Ridley. 2004. Ezrin/radixin/moesin proteins and Rho GTPase signalling in leucocytes. *Immunology.* 112:165–176.

3. Fehon, R. G., A. I. McClatchey, and A. Bretscher. 2010. Organizing the cell cortex: the role of ERM proteins. *Nat. Rev. Mol. Cell Biol.* 11:276–287.

4. Mangeat, P., C. Roy, and M. Martin. 1999. ERM proteins in cell adhesion and membrane dynamics. *Trends Cell Biol.* 9:187–192.

5. D'Angelo, R., S. Aresta, …, M. Arpin. 2007. Interaction of ezrin with the novel guanine nucleotide exchange factor PLEKHG6 promotes RhoG-dependent apical cytoskeleton rearrangements in epithelial cells. *Mol. Biol. Cell.* 18:4780–4793.

6. Prag, S., M. Parsons, …, T. Ng. 2007. Activated ezrin promotes cell migration through recruitment of the GEF Dbl to lipid rafts and preferential downstream activation of Cdc42. *Mol. Biol. Cell.* 18:2935–2948.

7. Lee, J. H., T. Katakai, …, A. Shimizu. 2004. Roles of p-ERM and Rho-ROCK signaling in lymphocyte polarity and uropod formation. *J. Cell Biol.* 167:327–337.

8. Rossy, J., M. C. Gutjahr, …, V. Niggli. 2007. Ezrin/moesin in motile Walker 256 carcinosarcoma cells: signal-dependent relocalization and role in migration. *Exp. Cell Res.* 313:1106–1120.

9. Lorentzen, A., J. Bamber, …, C. J. Marshall. 2011. An ezrin-rich, rigid uropod-like structure directs movement of amoeboid blebbing cells. *J. Cell Sci.* 124:1256–1267.

10. Kunda, P., A. E. Pelling, …, B. Baum. 2008. Moesin controls cortical rigidity, cell rounding, and spindle morphogenesis during mitosis. *Curr. Biol.* 18:91–101.

11. Carreno, S., I. Kouranti, …, F. Payre. 2008. Moesin and its activating kinase Slik are required for cortical stability and microtubule organization in mitotic cells. *J. Cell Biol.* 180:739–746.

12. Luxenburg, C., H. A. Pasolli, …, E. Fuchs. 2011. Developmental roles for Srf, cortical cytoskeleton and cell shape in epidermal spindle orientation. *Nat. Cell Biol.* 13:203–214.

13. Kunda, P., N. T. Rodrigues, E. Moeendarbary, T. Liu, A. Ivetic, G. Charras, and B. Baum. 2012. PP1-mediated moesin dephosphorylation couples polar relaxation to mitotic exit. *Current biology: CB.* 22:231–236.

14. Roubinet, C., B. Decelle, …, S. Carreno. 2011. Molecular networks linked by Moesin drive remodeling of the cell cortex during mitosis. *J. Cell Biol.* 195:99–112.

15. Berryman, M., R. Gary, and A. Bretscher. 1995. Ezrin oligomers are major cytoskeletal components of placental microvilli: a proposal for their involvement in cortical morphogenesis. *J. Cell Biol.* 131:1231–1242.

16. Gautreau, A., D. Louvard, and M. Arpin. 2000. Morphogenic effects of ezrin require a phosphorylation-induced transition from oligomers to monomers at the plasma membrane. *J. Cell Biol.* 150:193–203.

17. Zhu, L., Y. Liu, and J. G. Forte. 2005. Ezrin oligomers are the membrane-bound dormant form in gastric parietal cells. *Am. J. Physiol. Cell Physiol.* 288:C1242–C1254.

18. Barret, C., C. Roy, …, V. Niggli. 2000. Mutagenesis of the phosphatidylinositol 4,5-bisphosphate (PIP$_2$) binding site in the NH$_2$-terminal domain of ezrin correlates with its altered cellular distribution. *J. Cell Biol.* 151:1067–1080.

19. Yonemura, S., T. Matsui, …, S. Tsukita. 2002. Rho-dependent and -independent activation mechanisms of ezrin/radixin/moesin proteins: an essential role for polyphosphoinositides in vivo. *J. Cell Sci.* 115:2569–2580.

20. Wald, F. A., A. S. Oriolo, …, P. J. Salas. 2008. Atypical protein kinase Cι activates ezrin in the apical domain of intestinal epithelial cells. *J. Cell Sci.* 121:644–654.

21. Fievet, B. T., A. Gautreau, …, M. Arpin. 2004. Phosphoinositide binding and phosphorylation act sequentially in the activation mechanism of ezrin. *J. Cell Biol.* 164:653–659.

22. Bretscher, A., K. Edwards, and R. G. Fehon. 2002. ERM proteins and merlin: integrators at the cell cortex. *Nat. Rev. Mol. Cell Biol.* 3:586–599.

23. Hao, J. J., Y. Liu, …, S. Shaw. 2009. Phospholipase C-mediated hydrolysis of PIP2 releases ERM proteins from lymphocyte membrane. *J. Cell Biol.* 184:451–462.

24. Coscoy, S., F. Waharte, …, F. Amblard. 2002. Molecular analysis of microscopic ezrin dynamics by two-photon FRAP. *Proc. Natl. Acad. Sci. USA.* 99:12813–12818.

25. Fritzsche, M., A. Lewalle, …, G. Charras. 2013. Analysis of turnover dynamics of the submembranous actin cortex. *Mol. Biol. Cell.* 24:757–767.

26. Clark, A. G., K. Dierkes, and E. K. Paluch. 2013. Monitoring actin cortex thickness in live cells. *Biophys. J.* 105:570–580.

27. Cameron, L. A., B. R. Houghtaling, and G. Yang. 2011. Fluorescent speckle microscopy. *Cold Spring Harb. Protoc.* 2011:pdb top106.

28. Cunningham, C. C. 1995. Actin polymerization and intracellular solvent flow in cell surface blebbing. *J. Cell Biol.* 129:1589–1599.

29. Watanabe, N., and T. J. Mitchison. 2002. Single-molecule speckle analysis of actin filament turnover in lamellipodia. *Science.* 295:1083–1086.

30. Wagner, M. L., and L. K. Tamm. 2001. Reconstituted syntaxin1a/SNAP25 interacts with negatively charged lipids as measured by lateral diffusion in planar supported bilayers. *Biophys. J.* 81:266–275.

31. Goehring, N. W., D. Chowdhury, …, S. W. Grill. 2010. FRAP analysis of membrane-associated proteins: lateral diffusion and membrane-cytoplasmic exchange. *Biophys. J.* 99:2443–2452.

32. Kapitza, H. G., G. McGregor, and K. A. Jacobson. 1985. Direct measurement of lateral transport in membranes by using time-resolved spatial photometry. *Proc. Natl. Acad. Sci. USA.* 82:4122–4126.

33. Axelrod, D., D. E. Koppel, …, W. W. Webb. 1976. Mobility measurement by analysis of fluorescence photobleaching recovery kinetics. *Biophys. J.* 16:1055–1069.

34. Michelot, A., and D. G. Drubin. 2011. Building distinct actin filament networks in a common cytoplasm. *Current biology: CB.* 21:R560–R569.

35. Haggie, P. M., J. K. Kim, …, A. S. Verkman. 2006. Tracking of quantum dot-labeled CFTR shows near immobilization by C-terminal PDZ interactions. *Mol. Biol. Cell.* 17:4937–4945.

36. Zhu, L., R. Zhou, …, J. G. Forte. 2007. High turnover of ezrin T567 phosphorylation: conformation, activity, and cellular function. *Am. J. Physiol. Cell Physiol.* 293:C874–C884.

37. Hochmuth, F. M., J. Y. Shao, …, M. P. Sheetz. 1996. Deformation and flow of membrane into tethers extracted from neuronal growth cones. *Biophys. J.* 70:358–369.

38. Marcus, W. D., and R. M. Hochmuth. 2002. Experimental studies of membrane tethers formed from human neutrophils. *Ann. Biomed. Eng.* 30:1273–1280.

39. Charras, G. T., M. Coughlin, …, L. Mahadevan. 2008. Life and times of a cellular bleb. *Biophys. J.* 94:1836–1853.